

# Apocalmodulin Itself Promotes Ion Channel Opening and $\text{Ca}^{2+}$ Regulation

Paul J. Adams,<sup>1</sup> Manu Ben-Johny,<sup>1</sup> Ivy E. Dick,<sup>1</sup> Takanari Inoue,<sup>2,3</sup> and David T. Yue<sup>1,\*</sup>

<sup>1</sup>Calcium Signals Laboratory, Departments of Biomedical Engineering and Neuroscience, Center for Cell Dynamics, The Johns Hopkins University School of Medicine, 720 Rutland Avenue, Baltimore, MD 21205, USA

<sup>2</sup>Department of Cell Biology and Center for Cell Dynamics, The Johns Hopkins University School of Medicine, 855 N. Wolfe Street, Baltimore, MD 21205, USA

<sup>3</sup>Precursory Research for Embryonic Science and Technology, Japan Science and Technology Agency, 4-1-8 Honcho Kawaguchi, Saitama 332-0012, Japan

\*Correspondence: [dyue@jhmi.edu](mailto:dyue@jhmi.edu)

<http://dx.doi.org/10.1016/j.cell.2014.09.047>

## SUMMARY

The  $\text{Ca}^{2+}$ -free form of calmodulin (apoCaM) often appears inert, modulating target molecules only upon conversion to its  $\text{Ca}^{2+}$ -bound form. This schema has appeared to govern voltage-gated  $\text{Ca}^{2+}$  channels, where apoCaM has been considered a dormant  $\text{Ca}^{2+}$  sensor, associated with channels but awaiting the binding of  $\text{Ca}^{2+}$  ions before inhibiting channel opening to provide vital feedback inhibition. Using single-molecule measurements of channels and chemical dimerization to elevate apoCaM, we find that apoCaM binding on its own markedly upregulates opening, rivaling the strongest forms of modulation. Upon  $\text{Ca}^{2+}$  binding to this CaM, inhibition may simply reverse the initial upregulation. As RNA-edited and -spliced channel variants show different affinities for apoCaM, the apoCaM-dependent control mechanisms may underlie the functional diversity of these variants and explain an elongation of neuronal action potentials by apoCaM. More broadly, voltage-gated Na channels adopt this same modulatory principle. ApoCaM thus imparts potent and pervasive ion-channel regulation.

## INTRODUCTION

Calmodulin (CaM) lacking bound  $\text{Ca}^{2+}$  (apocalmodulin, apoCaM) has often been categorized as less capable of modulating target molecules, compared to CaM loaded with  $\text{Ca}^{2+}$  ( $\text{Ca}^{2+}$ /CaM) (Alberts et al., 1994). Certainly, there have been exceptions to this premise (Jurado et al., 1999), but CaM regulation of ion channels has seemingly followed the traditional order (Saimi and Kung, 2002). This study argues to the contrary for voltage-gated  $\text{Ca}^{2+}$  and Na channels.

Among the most salient examples of CaM modulation are those involving L type ( $\text{Ca}_v1.3$ )  $\text{Ca}^{2+}$  channels. These transport molecules serve as a dominant  $\text{Ca}^{2+}$  entry pathway into pace-making cardiomyocytes and neurons (Bean, 2007) and figure crucially in rhythmic functions like cardiac pacemaking and mo-

tor control involving substantia nigra, the prime neurodegenerative locus in Parkinson's (Chan et al., 2007; Obeso et al., 2008). As these channels convey substantial  $\text{Ca}^{2+}$  entry in these settings, modulation of  $\text{Ca}_v1.3$  is critical for  $\text{Ca}^{2+}$  signaling and homeostasis in health and disease (Bean, 2007; Chan et al., 2007; Puopolo et al., 2007).

One better-studied form of  $\text{Ca}_v1.3$  regulation is the  $\text{Ca}^{2+}$ -dependent inactivation (CDI) of this channel type by CaM (Evans and Zamponi, 2006). At first glance, the operation of CDI may now seem simple in coarse outline, at least for the best-studied  $\text{Ca}_v1.3$  channel variant (Ben-Johny and Yue, 2014). This “archetypical” form is distinguished by an IQ CaM-binding domain containing the sequence isoleucine-glutamine-aspartate-tyrosine (IQDY), followed by a stop codon soon after (Figure 1A, variant 0). A single  $\text{Ca}^{2+}$ -free CaM molecule (apoCaM) first preassociates with sites including the IQ domain (Figure 1B, configuration A), thus becoming a resident, but presumably dormant,  $\text{Ca}^{2+}$  sensor poised for subsequent channel regulation (Bazzazi et al., 2013; Ben-Johny et al., 2013; Erickson et al., 2003; Liu et al., 2010; Pitt et al., 2001).  $\text{Ca}^{2+}$  binding to this onboard apoCaM then sharply reduces channel open probability ( $P_o$ ) (Figure 1B, configuration I) (Ben-Johny et al., 2013), furnishing  $\text{Ca}^{2+}$ -negative feedback crucial for  $\text{Ca}^{2+}$  handling. Channels without apoCaM cannot undergo CDI (Bazzazi et al., 2013; Ben-Johny et al., 2013; Liu et al., 2010).

That said, the full reality of the modulatory landscape is staggering in its complexity, given recent discoveries of a prominent array of RNA-edited and splice variants of  $\text{Ca}_v1.3$  (rest of Figure 1A). RNA editing yields different sequences in the IQ element (Huang et al., 2012), and alternative splicing produces channels with conspicuous extensions after the IQ domain (Bock et al., 2011; Hui et al., 1991; Tan et al., 2011; Xu and Lipscombe, 2001). These newly recognized variants actually constitute the bulk of  $\text{Ca}_v1.3$  channels in the brain, and they exhibit vast differences in CDI (Bazzazi et al., 2013; Bock et al., 2011; Huang et al., 2012; Tan et al., 2011), projecting this diversity as an extensive but largely unexplored system for tuning  $\text{Ca}^{2+}$  dynamics. But CDI tuning may only foreshadow a larger mysterious effect—heterologous expression of  $\text{Ca}_v1.3$  variants frequently exhibits sharply diminished current densities that seem too prominent to attribute to happenstance (Bazzazi et al., 2013; Bock et al., 2011; Huang et al., 2012; Tan et al., 2011). Could a major

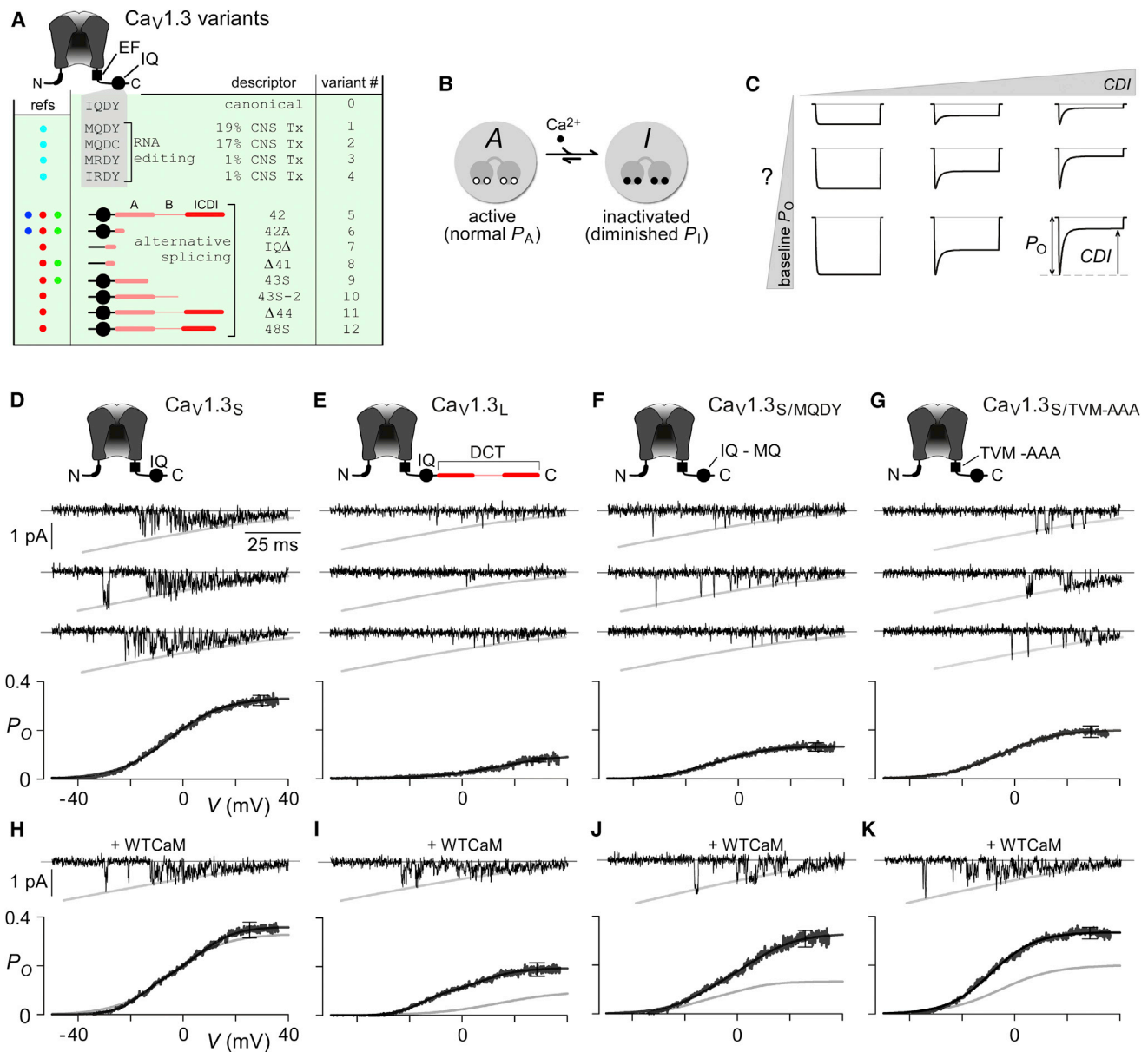


**Figure 1. CaM Alters  $P_O$  of L Type Channel Variants at Single-Molecule Level**

(A) Ca<sub>v</sub>1.3 channel carboxy-tail variation by alternative splicing and RNA editing. Cyan, blue, red, and green symbols correspond, respectively, to references Huang et al., 2012; Hui et al., 1991; Tan et al., 2011; and Bock et al., 2011.

(B) Configuration A (active), channels (shown as gray circles) bound to apoCaM (shown as two lobes and linker) have high baseline  $P_O$  ( $P_A$ ). Configuration I (inactivated), channels bound to Ca<sup>2+</sup>-CaM have diminished channel  $P_O$  ( $P_I$ ) (Ben-Johny et al., 2013; Imredy and Yue, 1994).

(C) Hypothetical fixed and idiosyncratic CDI and baseline  $P_O$  profiles for Ca<sub>v</sub>1.3 variants.

(D–G) Single-channel analysis of four recombinant Ca<sub>v</sub>1.3 variants transiently expressed in HEK293 cells with only endogenous CaM present. Top subpanels, unitary Ba<sup>2+</sup> currents during voltage ramp, shown between –50 mV and +40 mV (slanted gray lines, GHK fit). Bottom subpanel, average single-channel  $P_O$  versus voltage.

(H–K) Single-channel records under elevated apoCaM. Light gray line reproduced from corresponding variant above.

All averages derived from multiple patches ( $n = 4–6$ ). Error bars are  $\pm$  SEM throughout. Behaviors shown for Ca<sub>v</sub>1.3<sub>S</sub> (Extended Experimental Procedures for detailed sequence) in (A) and (D) were indistinguishable in this regard to those for a closely similar natural splice variant Ca<sub>v</sub>1.3<sub>42A</sub> (Xu and Lipscombe, 2001) (not shown).

unsuspected action of Ca<sub>v</sub>1.3 variation be to adjust baseline channel  $P_O$ , thereby producing an equally large or greater effect on Ca<sup>2+</sup> signaling than CDI? Figure 1C cartoons the potential

array of channel behaviors that would then result, where each hypothetical Ca<sup>2+</sup> current trace portrays the functional profile of an individual variant. Whether such  $P_O$  effects actually exist across

variants and whether their mechanistic underpinnings relate to CDI remain open and difficult questions that cloud the physiology and pharmacological manipulation of  $\text{Ca}_v1.3$  variant channels in relation to  $\text{Ca}^{2+}$  signaling and dysregulation.

Here, we exploit single-molecule and chemical-biological approaches to reveal a simple principle that may unify the spectrum of  $\text{Ca}_v1.3$  molecular variants. In particular, we combine chemical-dimerizer-driven step increases in plasmalemmal CaM with simultaneous electrophysiological readouts of channel function (Luik et al., 2008; Spencer et al., 1993; Suh et al., 2006). We thus reveal that the binding of a single apoCaM to channels does considerably more than permit CDI to occur. ApoCaM binding itself also enhances channel opening ( $P_O$ ) by several fold, rivaling the strongest forms of channel modulation (Miriayala et al., 2008). RNA editing, alternative splicing, and fluctuating CaM levels thus regulate CDI and baseline  $P_O$ , acting to variably populate pools of channels lacking or bound to apoCaM.

A key prediction is that elevated CaM should boost  $\text{Ca}_v1.3$  opening and prolong neuronal action potentials. Indeed, we explicitly demonstrate this outcome in substantia nigral neurons. More broadly, a recent study reveals notable similarity between the  $\text{Ca}^{2+}$ /CaM regulation of  $\text{Ca}_v$  channels and that of voltage-gated  $\text{Na}_v$  channels (Ben-Johny et al., 2014). Here, we generalize this likeness, showing that apoCaM binding to  $\text{Na}_v$  channels also strongly amplifies  $P_O$ . Thus, apoCaM imparts a potent and pervasive form of ion-channel regulation, whose implications range as far as the sweep of  $\text{Ca}_v$  and  $\text{Na}_v$  superfamilies, and perhaps beyond (Saimi and Kung, 2002).

## RESULTS

### CaM Modulates Baseline Opening of L Type Channels

We first tested whether the baseline  $P_O$  of certain variant channels is in fact diminished, and whether CaM at all influences this  $P_O$ . Figure 1D displays the properties of the canonical  $\text{Ca}_v1.3$  “short” splice variant ( $\text{Ca}_v1.3_S$ , Figure 1A, variant “0”), with the IQ domain translated as amino acids IQDY (as coded by genomic sequence). We used low-noise electrophysiology (Tay et al., 2012) to directly observe single-channel  $P_O$  and employed  $\text{Ba}^{2+}$  as the charge carrier through channels because  $\text{Ba}^{2+}$  binds poorly to CaM (Chao et al., 1984). This maneuver would thus preclude entry into configuration I (Figure 1B), allowing alterations in baseline  $P_O$  to be observed apart from CDI. Accordingly, a slow voltage ramp (shown from  $-50$  to  $+40$  mV) elicits stochastic openings that reflect near steady-state  $P_O$  at each voltage. The top rows display stochastic records, where channel closures correspond to the zero-current portions of the trace (on horizontal gray lines) and openings to downward deflections to the open level (slanted gray curves). Averaging many records yields a mean current that can be divided into the open level (slanted gray curve) to furnish the  $P_O$  versus voltage relation (sigmoidal trace at bottom), averaged over multiple patches.

Thus appraised, we examined the single-molecule properties of a prominently expressed  $\text{Ca}_v1.3$  “long” splice variant (variant 5 in Figure 1A), featuring an extended distal carboxyl tail (DCT) as schematized atop Figure 1E. For convenience, we will refer to this variant as  $\text{Ca}_v1.3_L$ . Scrutiny of the single-trial records and

$P_O$ -V relation for this variant indeed reveals a far lower  $P_O$ . Interestingly, the presence of a DCT is not required for a diminished  $P_O$  because Figure 1F shows that a common RNA-edited variant within a short-splice configuration (variant 1 in Figure 1A, or  $\text{Ca}_v1.3_{S/MQDY}$ ) also displays attenuated  $P_O$  compared to the canonical  $\text{Ca}_v1.3_S$ . Curiously, both  $\text{Ca}_v1.3_L$  and  $\text{Ca}_v1.3_{S/MQDY}$  exhibit diminished apoCaM binding affinity (Bazzazi et al., 2013; Liu et al., 2010). Thus, we tested for  $P_O$  effects in a man-made variant, where apoCaM affinity has been attenuated by mutations in the carboxyl tail of  $\text{Ca}_v1.3_S$  ( $\text{Ca}_v1.3_{S/TVM-AAA}$ , cartooned atop Figure 1G) (Ben-Johny et al., 2013).  $\text{Ca}_v1.3_{S/TVM-AAA}$  also exhibits reduced  $P_O$  (Figure 1G).

Given this pattern, we tested more directly for the involvement of apoCaM in modulating  $P_O$ , by strongly overexpressing recombinant CaM with these same constructs. Perhaps,  $P_O$  might be upregulated by apoCaM occupancy of some site, so that overexpressing CaM may boost occupancy by mass action. For the prototypic short variant  $\text{Ca}_v1.3_S$ , no such enhancement of  $P_O$  is produced by CaM overexpression (Figure 1H), as if the hypothetical site were already bound to CaM at baseline. By contrast, elevated CaM produces an impressive increase of  $P_O$  in all other constructs with diminished apoCaM affinity (Figures 1I–1K), where an appreciable fraction of channels might initially lack indwelling CaM.

### Single-Channel $P_O$ Modulated in Quantized Manner

However, overexpressing recombinant CaM could enhance channel  $P_O$  by a multitude of mechanisms besides binding to a channel modulatory site. For example, CaM-dependent modulation of various kinases and phosphatases or even gene regulation of auxiliary factors could be in play (Bers and Grandi, 2009). To garner further mechanistic constraints, we considered a distinctive feature of an apoCaM-binding model, as diagrammed atop Figure 2A. Here, beyond the configuration A described earlier, we explicitly hypothesize a configuration lacking apoCaM at a  $P_O$  modulatory site (configuration E). In this formulation, channels bound to apoCaM (configuration A) would open with a high  $P_O$  as exemplified by  $\text{Ca}_v1.3_S$  (Figure 1D), and those lacking apoCaM would exhibit low  $P_O$ . A hallmark feature of this paradigm is that channel  $P_O$  should be quantized, manifesting as a high  $P_O$  “mode of channel gating” when apoCaM is bound (Hess et al., 1984) or a low  $P_O$  mode when apoCaM is absent. By contrast, many other mechanisms (e.g., multiple phosphorylation sites) could produce a graded spectrum of intermediate effects. These contrasts might be abundantly clear at the single-channel level.

Figure 2A displays twelve sequential single-channel trials of the RNA-editing variant  $\text{Ca}_v1.3_{S/MQDY}$  with only endogenous CaM present. Activity was evoked by voltage ramps introduced at 12 s intervals. The activity appears uniformly sparse, as confirmed by the diary plot of average  $P_O$  within individual trials ( $\bar{P}_O$ , Figure 2B), as well as the single bell-shaped distribution of  $\bar{P}_O$  drawn from a larger set of trials (Figure 2D). These results are consistent with a channel residing almost exclusively within a hypothesized configuration E. The corresponding average  $P_O$ -V relation (Figure 2C) may thus pertain to channels residing in configuration E alone.

By contrast, upon strongly coexpressing recombinant CaM with another  $\text{Ca}_v1.3_{S/MQDY}$  channel (Figures 2E–2H), activity is

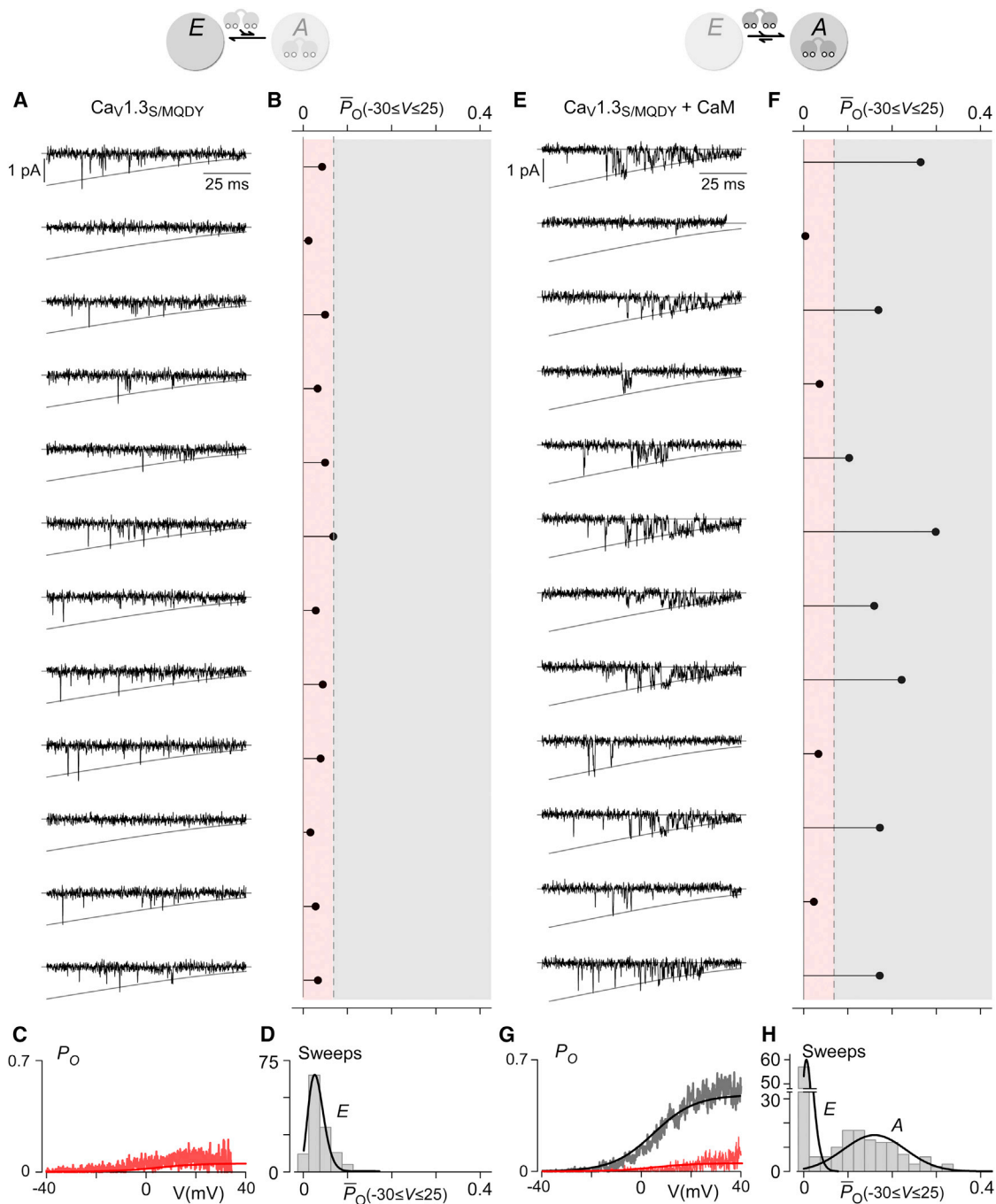


**Figure 2. Single-Channel  $P_O$  Modulated by CaM in Quantized Manner**

(A)  $\text{Ca}_v1.3\text{S/MQDY}$  in HEK cells with only endogenous CaM present; mainly expected to occupy configuration *E* (top cartoon). Single-channel  $\text{Ba}^{2+}$  currents during voltage ramp, shown between  $-40$  and  $+40$  mV, elicited at 12 s intervals.

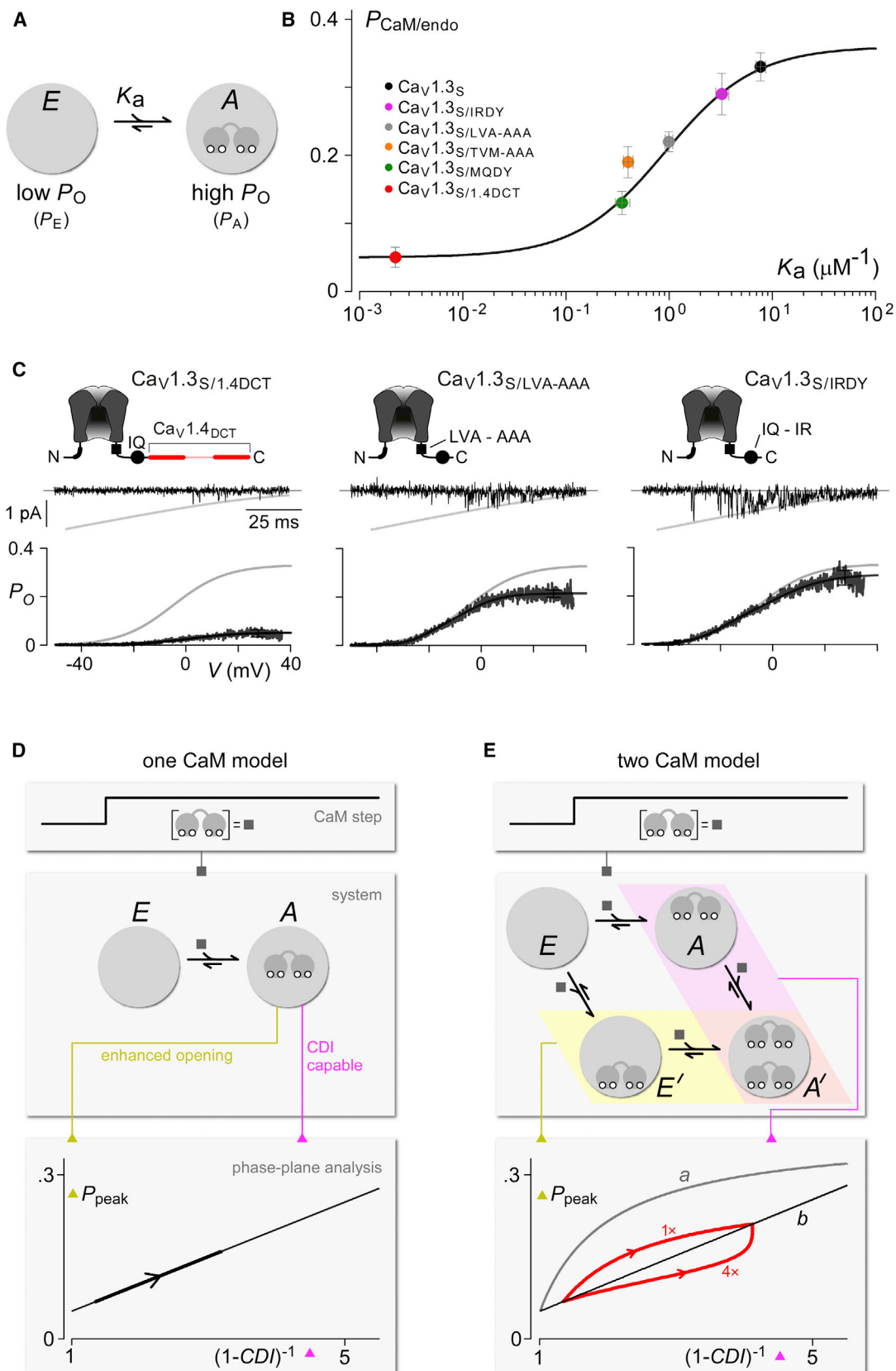
(B) For each current trace in (A), average  $P_O$  between  $-30$  and  $+25$  mV ( $\bar{P}_O(-30 \leq V \leq 25)$ ) was calculated. Traces categorized into low  $P_O$  (red-shaded) region or high  $P_O$  range (gray-shaded).

(C) Average  $P_O$  at each voltage, calculated separately for traces in low  $P_O$  (red) versus high  $P_O$  range (gray). In this case, all traces are in low  $P_O$  group (red).

(D) Number of sweeps with  $\bar{P}_O(-30 \leq V \leq 25)$  within indicated  $P_O$  ranges. Histogram fits with unimodal distribution ( $p > 0.9$ ) by Hartigan's dip test (Extended Experimental Procedures).

(E–H) Same analysis for  $\text{Ca}_v1.3\text{S/MQDY}$  with CaM overexpression. (H)  $\bar{P}_O$  histogram unlikely to be unimodal ( $p < 0.05$ , Hartigan's dip test), thus fit by bimodal distribution.

See also Figures S1 and S2.



(legend on next page)



markedly enhanced in a conspicuously quantized manner. Although many trials exhibit a high  $P_O$  pattern of gating (Figure 2E, trials 1, 3, 5–8, 10, 12), low  $P_O$  trials resembling those without apoCaM overexpression (Figure 2A) are clearly interspersed (Figure 2E, trials 2, 4, 9, 11). This apparent quantization of high and low  $P_O$  gating is confirmed by the segregation of  $\bar{P}_O$  into distinct zones in the diary plot (Figure 2F) and by the bimodal distribution of  $\bar{P}_O$  amassed from a large number of trials (Figure 2H). Little intermediate activity can be discerned. These data are thus consistent with channel switching between discrete  $E$  and  $A$  configurations. By grouping trials into high and low  $P_O$  groups with the dashed-line discriminator in Figure 2F, we could estimate separate  $P_O$ - $V$  relations for each gating mode (Figure 2G). Notably, the low  $P_O$ - $V$  relation (red) is fit by the same function used without elevating apoCaM (Figure 2C), arguing for the invariance of configuration  $E$  between conditions. Also notable is the  $\sim 7$ -fold enhancement of high versus low  $P_O$ - $V$  relations, suggesting an enormous effect of apoCaM on channel opening. Parallel experiments with other  $\text{Ca}_v1.3$  variant channels ( $\text{Ca}_v1.3_S$ ,  $\text{Ca}_v1.3_L$ ,  $\text{Ca}_v1.3_{\text{TVM-AAA}}$ ) confirmed similar quantized behavior (Figures S1 and S2).

### ApoCaM Binding to CDI Site Correlates with Enhanced Baseline $P_O$

The digital manner by which apoCaM enhances baseline  $P_O$  fits well with a simple apoCaM-binding mechanism (top of Figure 2). Nonetheless, other plausible mechanisms could also elaborate quantized behavior, such as phosphorylation and dephosphorylation at a single site. To begin to discriminate among these possibilities, we noted that a direct CaM-binding mechanism for  $P_O$  modulation (Figure 3A) would predict a simple Langmuir relation between the peak  $P_O$  measured with only endogenous apoCaM present ( $P_{\text{CaM/endo}}$ ) and the association constant for apoCaM binding to a presumed  $P_O$  modulatory site ( $K_a$ ). Figure S3 yields:

$$P_{\text{CaM/endo}} = P_E + (P_A - P_E) \cdot K_a / (K_a + \Lambda) \quad (1)$$

where  $P_E$  is the open probability of channels lacking apoCaM (Figure 3A, configuration  $E$ ),  $P_A$  the open probability of channels prebound to apoCaM (configuration  $A$ ), and  $\Lambda \propto [\text{apoCaM}_{\text{bulk}}]^{-1}$ .

The challenge with applying tests based on this equation was the unknown identity of the hypothetical apoCaM-binding site for  $P_O$  modulation, much less the corresponding  $K_a$  for various  $\text{Ca}_v1.3$  variants. Indeed, atomic structures of  $\text{Ca}^{2+}$ /CaM complexed with carboxy-tail peptides of closely related  $\text{Ca}_v1.2$  channels argue for the binding of multiple CaM molecules per tail, each bound CaM imparting a different function (Fallon et al., 2009; Kim et al., 2010). That said, we conjectured that the

apoCaM-binding site for  $P_O$  modulation might be one and the same as the site involved in the CDI process (Figure 1B). Elsewhere, we have previously determined the  $K_a$  values for apoCaM binding to the carboxy-tail site relating to CDI, not only for the  $\text{Ca}_v1.3$  variants in Figures 1E–1H but also for additional variants whose  $P_O$  profiles are characterized in Figure 3C (Bazzazi et al., 2013; Ben-Johny et al., 2013; Liu et al., 2010). Plotting  $P_{\text{CaM/endo}}$  versus  $K_a$  for all of these variants in Figure 3B then tests for the prediction of Equation 1. It is noteworthy how well the data symbols fit with the Langmuir function (smooth curve) in Figure 3B, an outcome consistent with the binding of one and the same apoCaM modulating both  $P_O$  and the ability to undergo CDI. For robustness, open probabilities were measured at maximal depolarization for the plot in Figure 3B.

### Rapid Plasmalemmal Recruitment of ApoCaM Triggers Dual Modulation of $P_O$ and CDI

Nonetheless, the suggestive correlation in Figure 3B requires compilation of data from several variants, characterized over multiple cells by differing techniques. By contrast, a considerably more direct test would arise if we could abruptly change the free apoCaM concentration at the cytoplasmic face of channels, all while performing electrophysiology within individual cells. The result would be revealing because the evolving values of CDI and  $P_O$  thus observed would adhere to a specific moment-to-moment interrelation if the one-apoCaM mechanism conjectured above were to hold true. This can be seen as follows in Figure 3D. The top subpanel portrays a hypothetical step-like increase in the free apoCaM concentration facing channels. This “input” would drive a scheme in which channel binding to a single apoCaM imparts a shift from configurations  $E$  to  $A$ , defined such that channels in  $E$  are incapable of undergoing CDI and exhibit a low  $P_O$  ( $P_E$ ), whereas those in  $A$  demonstrate a robust CDI and a high  $P_O$  ( $P_A$ ) before undergoing CDI. The following linear relation must then hold for a mixed population of channels, such as observed in whole-cell recordings (Figure S4),

$$I_{\text{peak}}/I_{\text{max}} = P_E \cdot (1 - \text{CDI})^{-1}, \quad (2)$$

where  $I_{\text{peak}}$  is the peak  $\text{Ca}^{2+}$  current before CDI onset;  $I_{\text{max}}$  is the current amplitude if all channels in a cell were simultaneously open;  $\text{CDI}$  is the CDI metric defined in Figure 1C; and  $P_E$  is the open probability of channels in configuration  $E$  ( $= 0.051$  from Figure 3C). In this relation,  $(1 - \text{CDI})^{-1}$  may be considered a linearized CDI metric, starting at one when  $\text{CDI}$  is absent, and growing larger as  $\text{CDI}$  intensifies. As well,  $I_{\text{peak}}/I_{\text{max}}$  turns out to be the average peak open probability of all channels in a cell before CDI onset, referred to as  $P_{\text{peak}}$ . That said, the thin black line in

### Figure 3. ApoCaM Affinity Tunes $P_O$

- (A) Proposal that channel apoCaM affinity ( $K_a$ ) specifies equilibrium between configurations  $E$  (low  $P_O$ ) and  $A$  (high  $P_O$ ).  
 (B) Plot of peak  $P_O$  obtained with only endogenous CaM present ( $P_{\text{CaM/endo}}$ ) versus previously estimated association constants gauged by live-cell FRET between channel carboxyl termini and apoCaM (Figure S3 and Table S1). Error bars are  $\pm$  SEM.  
 (C) Average  $P_O$  (format as in Figures 1E–1L) for recombinant  $\text{Ca}_v1.3_S$  channels with variant carboxyl tails yielding reduced apoCaM affinity. Gray lines from basic  $\text{Ca}_v1.3_S$  (Figure 1E) for comparison. All averages from multiple patches ( $n = 3$ –6). Error bars are  $\pm$  SEM.  
 (D) Phase-plane signature of single-CaM behavior during CaM transients.  
 (E) Two-CaM behavior during CaM transients, revealed by phase-plane paradigm.  
 See also Figure S4.

the bottom subpanel of Figure 3D explicitly plots Equation 2. Here, a key feature concerns the immutable interrelation between  $P_{\text{peak}}$  and  $(1 - \text{CDI})^{-1}$ , even during an abrupt increase of apoCaM. Even though apoCaM binding to channels would deviate from equilibrium during such a transition, all  $P_{\text{peak}}$  versus  $(1 - \text{CDI})^{-1}$  points would nonetheless reside on the same line (thick black arrow trajectory). This feature arises because each point on the trajectory corresponds to a specific fraction of channels bound to apoCaM, and each fraction enforces a unique pairing of  $P_{\text{peak}}$  versus  $(1 - \text{CDI})^{-1}$  values. In this scheme, then, there are no arrangements that fall outside this regime.

By contrast, if the enhancement of baseline  $P_O$  were governed by a separate process other than the apoCaM binding that arms channels for CDI, deviation from the linear relation in Figure 3D would likely occur. For concreteness, consider a system where apoCaM binding to one site enables CDI to proceed (Figure 3E, middle subpanel, configurations within magenta zone), but apoCaM binding to an alternative site (yielding configurations in yellow zone) increases baseline  $P_O$  before CDI onset, from  $P_E$  to  $P_A$ . For simplicity, apoCaM binding to these sites is assumed to occur independently, and the steady-state fraction of peak current remaining after CDI is set to reproduce the experimentally observed CDI in  $\text{Ca}_v1.3_S$  (Ben-Johny et al., 2013). If the dissociation constants for apoCaM binding to  $P_O$  ( $K_{d(P)}$ ) and CDI ( $K_{d(\text{CDI})}$ ) sites were equivalent, then the two-CaM scheme would predict the downwardly convex relation between  $P_{\text{peak}}$  and  $(1 - \text{CDI})^{-1}$  (Figure 3E, curve a in bottom subpanel), contrasting with the linear relation for the one-CaM scheme. However, if  $K_{d(\text{CDI})}$  were precisely equal to  $K_{d(P)} \cdot P_E / P_A$ , then the two-CaM scheme would still enforce the linear relation in the bottom subpanel of Figure 3E (curve b) at steady state, where this line would be identical to that for the one-CaM scheme (Figure S4). However, even here, the difference in dissociation constants at the two sites means that the transient response to abrupt changes in apoCaM would deviate from the linear steady-state relation; this outcome is demonstrated by the numerically simulated hysteretic trajectories in Figure 3E (red), where the CDI regulatory site loads at the same rate or faster than the  $P_O$  site as marked (Figure S4). In sum, this manner of analysis relating to abrupt changes in apoCaM furnishes powerful means to distinguish among differing mechanisms. Likewise, other potential  $P_O$  modulatory mechanisms, like channel phosphorylation, would predict analogous deviations from linearity (Equation 2), particularly during abrupt increases in apoCaM.

We therefore exploited chemical-biological step generation of apoCaM concentration at the cytoplasmic face of channels, based on rapamycin-triggered dimerization of cytoplasmic FK506-binding protein (FKBP) and the FKBP-rapamycin-binding protein (FRB) localized to plasmalemma by a signal sequence from Lyn kinase (Lyn-FRB) (Phua et al., 2012). Figure 4A cartoons the layout, where bath-applied rapamycin should sharply increase perimembranous apoCaM, as confirmed by confocal microscopy visualizing the FKBP-CaM moiety (Figure 4B, top). Line-histogram analysis reveals a 6-fold increase of perimembranous CaM with  $\tau \sim 20$  s (Suh et al., 2006) (Figure 4B, bottom). Hence, coexpressing  $\text{Ca}_v1.3$  variants in this context would permit electrophysiological readouts of  $P_O$  and CDI during periods of rapidly increasing apoCaM.

$\text{Ca}_v1.3_S$  serves as a control (Figure 4C). Because of its high apoCaM affinity at the CDI site, most channels here might already be charged with apoCaM at baseline, such that increasing apoCaM with rapamycin should produce negligible change. The top two rows display diary plots of peak current and CDI measured from  $\text{Ca}^{2+}$  currents evoked every 20 s by 30 mV step depolarizations, with corresponding current waveforms shown below. The baseline  $P_O$  of channels is proportional to peak current, which is displayed in a normalized format ( $I_{\text{peak}} / I_O$ , as defined below) to facilitate averaging across cells. The metric of CDI (CDI) is specified by  $I_{\Delta} / I_{\text{peak}}$ , with these measures also diagrammed below. As expected, augmentation of apoCaM concentration by rapamycin negligibly perturbed either metric.

By contrast, for an RNA-edited variant ( $\text{Ca}_v1.3_{S/\text{MQDY}}$ ) with moderate apoCaM affinity, a markedly different outcome arises (Figure 4D). Here, rapamycin-induced CaM enrichment causes a hand-in-hand increase of peak current and CDI, clearly evident in exemplar traces on the bottom. These trends are entirely corroborated by averaged diary plots above (green circles, top and middle rows). Similarly, parallel increases in peak current and CDI were observed for two other variants featuring reduced aggregate apoCaM affinity (Figures 4E and 4F), each with distinctive response kinetics to the step increase of apoCaM. As a control, parallel experiments performed without CaM fused to FKBP invariably showed no changes in either peak current or CDI upon application of rapamycin, verifying that the observed effects were due to CaM enrichment and not FKBP itself (Figure S5). Also, current densities for variants predicted to lack apoCaM at baseline (Figures 4D–4F) were on average smaller than for  $\text{Ca}_v1.3_S$  (Figure 4C), as would be expected if  $P_O$  were diminished without bound apoCaM (Figure S5E). Finally, recruiting a CaM mutant unable to bind  $\text{Ca}^{2+}$  ( $\text{CaM}_{1234}$ ), and using  $\text{Ba}^{2+}$  as the charge carrier, provided further evidence that apoCaM is in fact responsible for the observed enhancement in  $P_O$  (Figure S6).

### One CaM Augments Baseline $P_O$ and Enables CDI

With these well-behaved transient responses in hand, we undertook mechanistic analysis relating to moment-to-moment plots of  $P_{\text{peak}}$  versus  $(1 - \text{CDI})^{-1}$ . Figure 5A renders as dark green symbols the data from the exemplar cell in Figure 4D ( $\text{Ca}_v1.3_{S/\text{MQDY}}$ ), with explicit labeling of points (i, ii, and iii) corresponding to exemplar currents shown earlier. The only free parameter is  $I_{\text{max}}$  in Equation 2, which was adjusted only to vertically normalize the data. Accordingly, the observed linearity and correspondence to predicted slope  $P_E$  is intrinsic to the data set. Therefore, adherence of these data points, and those from additional cells (pale green symbols), to the one-CaM relation throughout the CaM step is significant. Applying the same analysis to data from the exemplar cell in Figure 4E ( $\text{Ca}_v1.3_L$ ) also demonstrates strict conformity to the same linear relation, even with numerous points drawn from the transient phase of the response (Figure 5B, dark blue symbols). Points from other cells (pale blue symbols) also adhere nicely to the same relation. Data for the exemplar cell relating to still another variant (Figure 4F,  $\text{Ca}_v1.3_{S/1.4\text{DCT}}$ ) also reside on the same line (Figure 5C, dark red symbols), and additional cells also conformed to the same line (pale red symbols). Finally, Figure 5D overlays all these

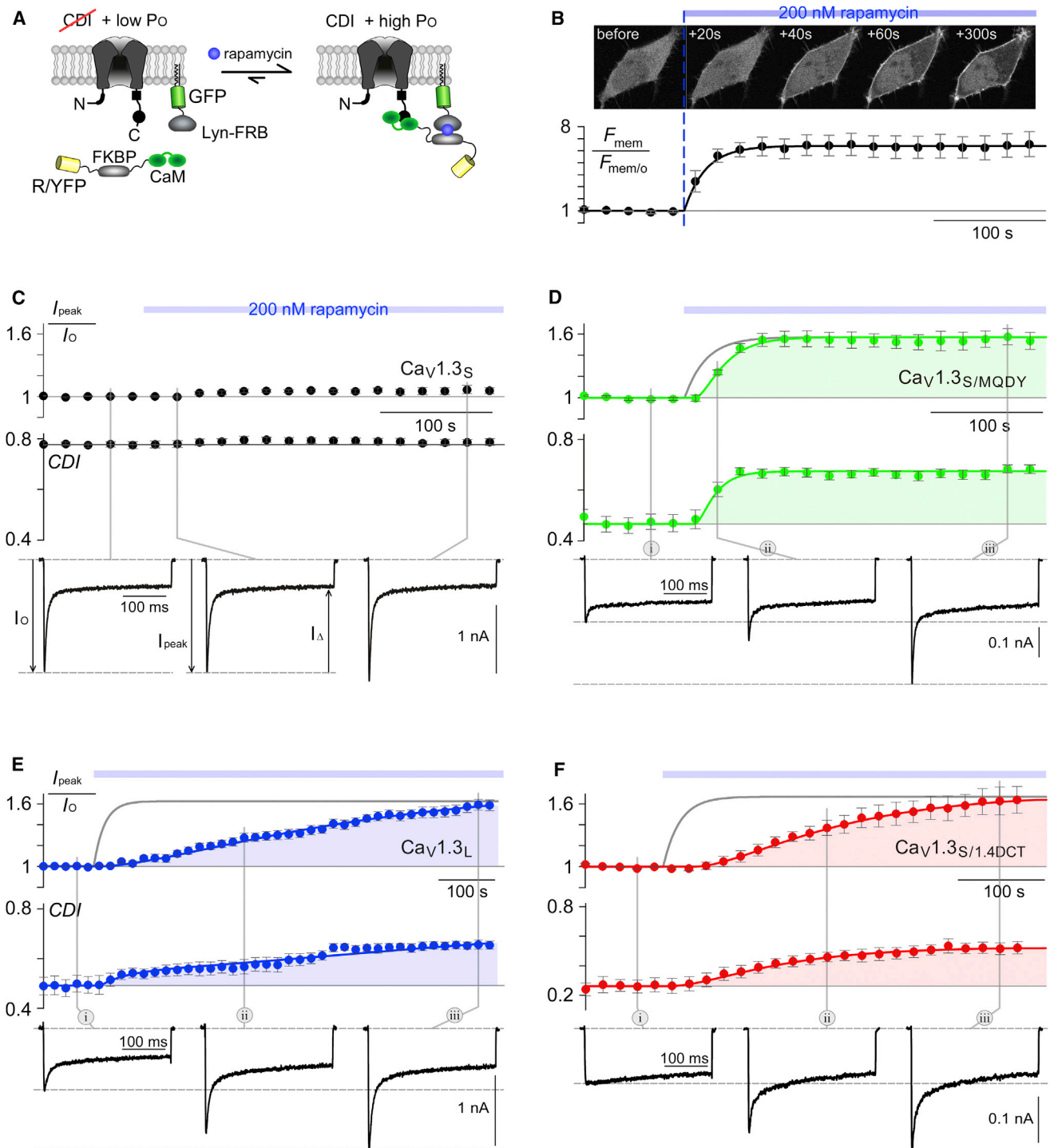


**Figure 4. Step Increases in CaM Rapidly Modulate Both Peak Current and CDI**

(A) Recombinant channels in HEK293 cells with both membrane-localized GFP-tagged FRB and cytosolic RFP/YFP-tagged FKBP fused to wild-type CaM. (B) Top, confocal image of RFP/FKBP/CaM translocation to plasma membrane on 200 nM rapamycin perfusion. Bottom, time course of RFP membrane fraction measured every 20 s ( $n = 7$  cells). (C) Diary of normalized peak current (top subpanel) and CDI (middle subpanel) from whole-cell  $Ca^{2+}$  currents through  $Ca_v1.3_s$  channels, evoked at 20 s intervals by steps to +30 mV from -90 mV holding potential. Corresponding current waveforms below. (D–F) Normalized peak current and CDI for  $Ca_v1.3$  variants with reduced apoCaM affinity. Format as in (C). Gray fit of apoCaM recruitment to plasmalemma from (B). All peak current and CDI measures obtained from multiple cells ( $n = 4–8$ ). Error bars are  $\pm$  SEM in (B)–(F). See also [Figures S5](#) and [S6](#).



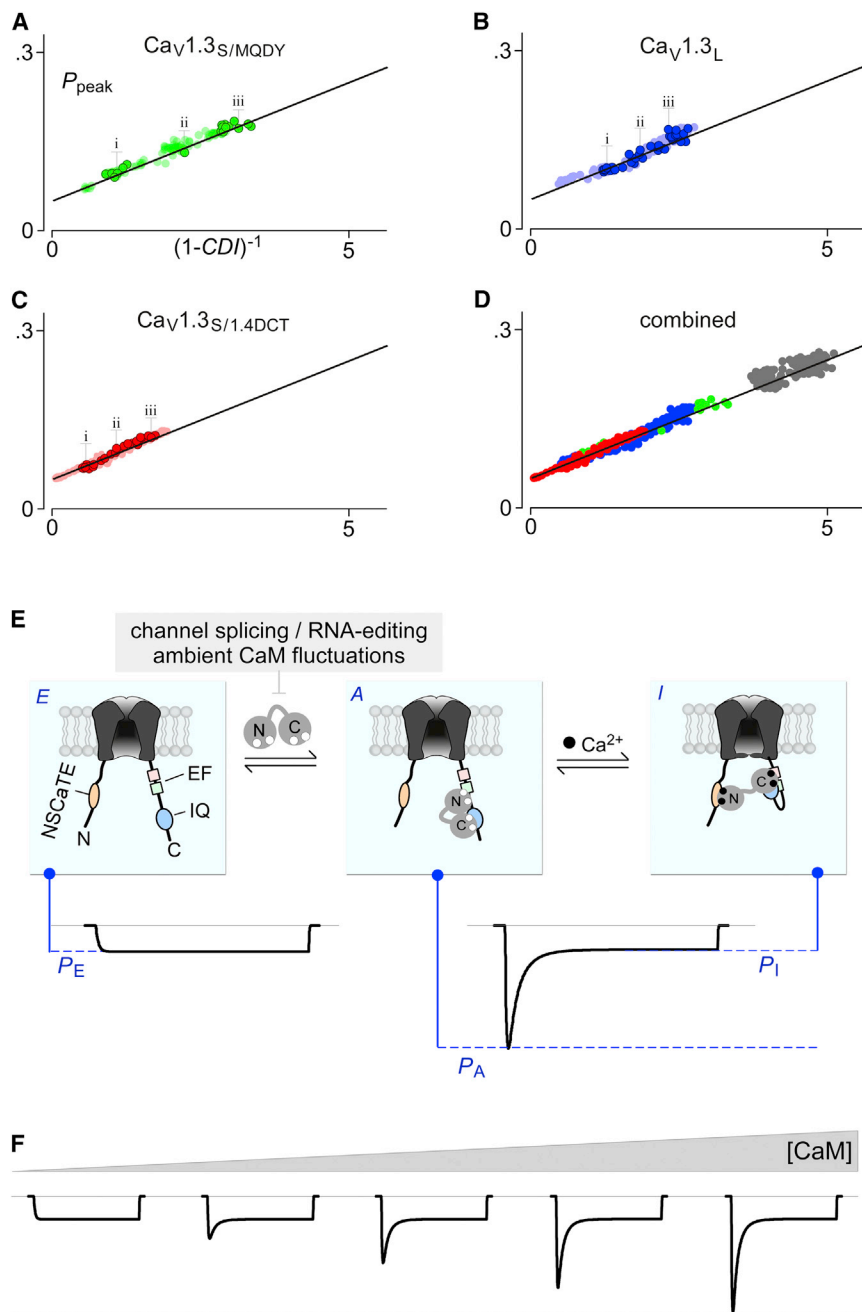


**Figure 5. Phase-Plane Analysis Indicates that One CaM Modulates Both  $P_O$  and CDI**

(A) Dark green symbols for exemplar cell in Figure 4D ( $\text{Ca}_v1.3_{\text{S/MQDY}}$ ), with labeled points (i, ii, and iii) corresponding to exemplar currents in Figure 4D. Pale green symbols, data from additional cells expressing  $\text{Ca}_v1.3_{\text{S/MQDY}}$ . (B and C) Same analysis for exemplar cells in Figure 4E ( $\text{Ca}_v1.3_{\text{L}}$ , dark blue symbols) and Figure 4F ( $\text{Ca}_v1.3_{\text{S/1.4DCT}}$ , dark red symbols), respectively. Pale symbols, data from additional cells. (D) Data from additional cells for each variant and for a further canonical  $\text{Ca}_v1.3_{\text{S}}$  variant (dark gray symbols) ( $n = 23$  cells). (E) One-apoCaM mechanism unifies diversity of baseline  $P_O$  and CDI properties of  $\text{Ca}_v1.3$  variants. (F) Simulation of  $P_O$ -CDI coordination with free apoCaM concentration for a single  $\text{Ca}_v1.3$  variant.

### Predicted Neuronal Action Potential Elongation

The strong upregulation of  $\text{Ca}_v1.3$  channel  $P_O$  by apoCaM promises significant consequences, particularly where  $\text{Ca}_v1.3$  channels contribute prominently to pacemaking, such as in the substantia nigral neurons modulating movement control (Chan et al., 2007; Christel et al., 2012; Obeso et al., 2008). Importantly, elevated  $\text{Ca}^{2+}$  in dopaminergic neurons in the substantia nigra pars compacta (SNc) predisposes for neurodegeneration in Parkinson's disease (Bezprozvanny, 2009).  $\text{Ca}_v1.3$  channels here support the bulk of  $\text{Ca}^{2+}$  entry (Bean, 2007; Cardozo and Bean, 1995; Chan et al., 2007; Puopolo et al., 2007), and  $\text{Ca}^{2+}$  channel activity shapes action potential (AP) morphology (Nedergaard, 1999; Puopolo et al., 2007). These neurons express a variety of  $\text{Ca}_v1.3$  splice and RNA-edited variants as shown in Figure 1A (Bock et al., 2011; Huang et al., 2012), and elevating CaM in these cells drives CaM onto low-affinity channel variants by mass action (Bazzazi et al., 2013). Numerical simulations described below predict

data, and those of another variant (gray symbols,  $\text{Ca}_v1.3_{\text{S}}$ ), thus arguing strongly for compliance with a single linear relation. On this basis, we propose the simple one-apoCaM mechanism in Figure 5E, which may unify the diversity of baseline  $P_O$  and CDI properties of numerous variants (Figure 1A). RNA-editing and splice variants modulate  $P_O$  and CDI over a large range, largely by tuning the affinity of apoCaM binding to channels (in configuration E), rather than by specialized molecular mechanisms particular to each variant. Fluctuations in ambient apoCaM could also tune  $\text{Ca}_v1.3$  as shown in Figure 5F. Two realms of generalization immediately follow.

that apoCaM enhancement of  $\text{Ca}_v1.3$  opening should produce telling changes in action-potential morphology, which we tested for experimentally as follows.

SNc dopaminergic neurons were dissected from transgenic mice selectively expressing GFP under the tyrosine hydroxylase (TH) promoter, enabling robust identification via fluorescence (Figure 6A, left subpanel). After culture for 1–7 days, cells maintained typical autonomous pacing at  $1.0 \pm 0.03$  Hz (middle subpanel) and AP morphology (right subpanel) (Chan et al., 2007; Grace and Bunney, 1984; Puopolo et al., 2007). The AP duration at 90% of baseline ( $\text{APD}_{90}$ ) was  $7.4 \pm 0.03$  ms, as expected from

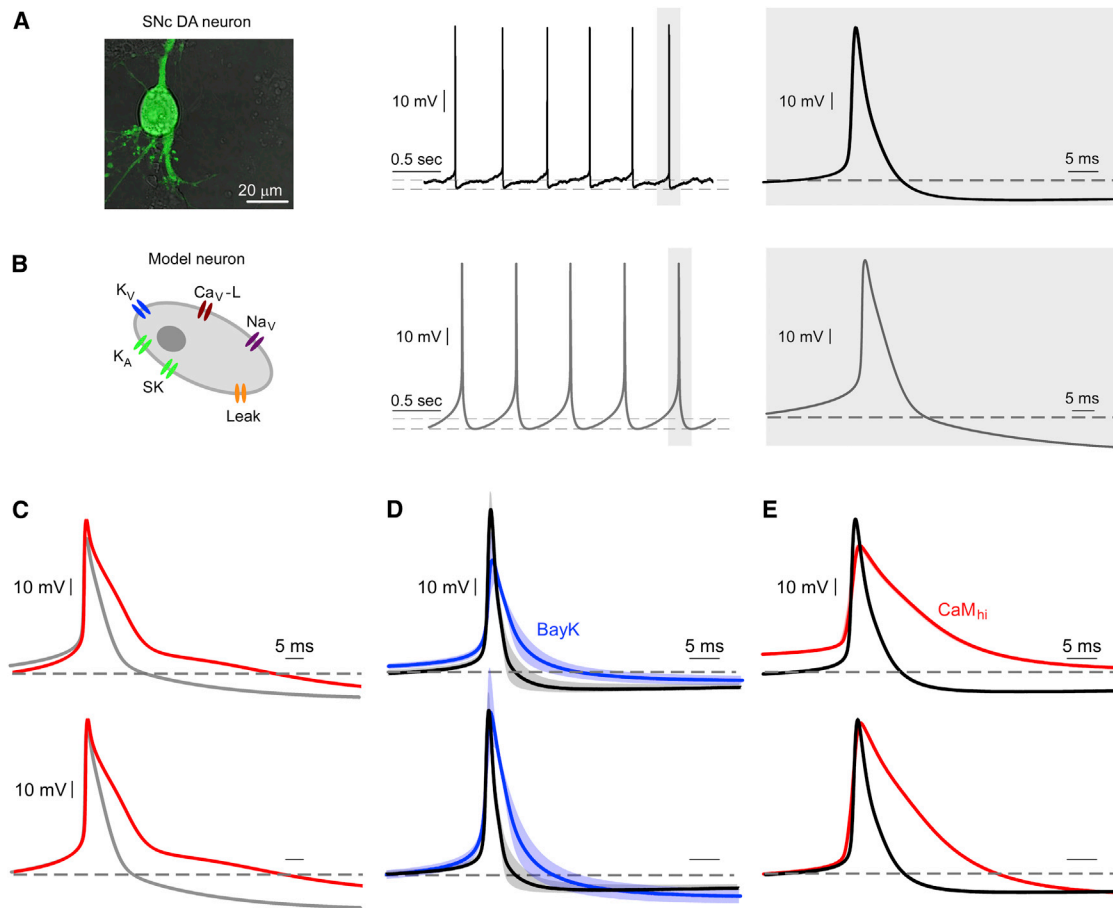


**Figure 6. Predicted AP Elongation in Neurons**

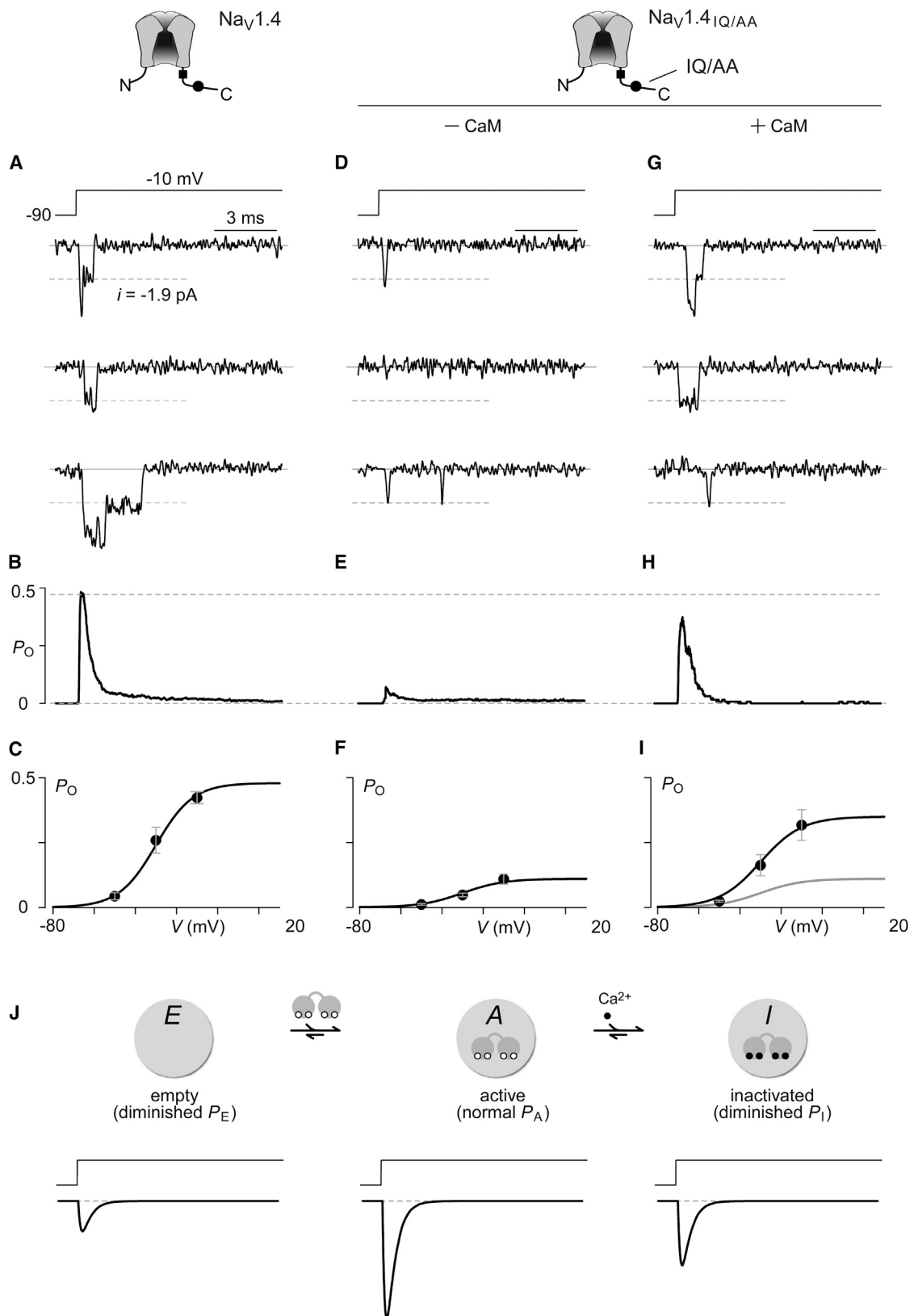
(A) Confocal image of cultured mouse substantia nigra (pars compacta) dopamine neuron (left subpanel). Middle subpanel, representative current-clamp recording of pacing in a SNc DA neuron in culture. Right subpanel, characteristic AP waveform obtained by averaging  $\sim 2,100$  APs. (B) Quantitative *in silico* model (left subpanel). Numerical simulations of pacing (middle subpanel) and AP morphology (right subpanel) are shown. (C) Simulated AP waveforms with fraction of  $\text{Ca}_v1.3$  channels bound to apoCaM equal to 0.3 (gray), compared to fraction bound of unity (red). Top subpanel, raw waveforms; bottom subpanel, normalized waveforms. See [Extended Experimental Procedures](#) and [Table S2](#). (D) Average AP from cultured SNc DA neurons before (black trace), and after applying Bay K8644 (5  $\mu\text{M}$ ) (blue trace) ( $n > 620$  APs). (E) AP recorded in SNc DA neurons with only endogenous CaM present (black trace) and with CaM overexpression (red trace) ( $n > 800$  APs). All APs measured from  $n = 4$ –5 cells. SEM shown as shading in (D) and (E).

prior reports (Puopolo et al., 2007). To predict the effects of apoCaM-driven  $P_O$  enhancement on AP morphology, we performed *in silico* simulations with a model (Chan et al., 2007) that closely recapitulated the firing pattern and AP morphology of these cultured neurons (Figure 6B) (Extended Experimental Procedures). Upon increasing the fraction of  $\text{Ca}_v1.3$  channels bound to CaM by 3-fold, simulated AP waveforms elongate dramatically from the gray baseline trace to the red waveform (Figure 6C). The top subpanel displays raw waveforms, and the bottom subpanel normalizes these responses to facilitate visual comparison of durations. Current-clamp records in cultured neurons confirmed that enhancement of L type channel  $P_O$  by Bay K8644 induced similar AP prolongation, with  $\text{APD}_{90}$  increasing from  $4.9 \pm 0.92$  to  $11.5 \pm 1.55$  ms (Figure 6D). The key test came with lentiviral-mediated overexpression of wild-type CaM, yielding a striking increase of  $\text{APD}_{90}$  from  $7.4 \pm 0.03$  ms with endogenous CaM to

$24.3 \pm 0.40$  ms on overexpressing CaM (Figure 6E). Thus, fluctuations of apoCaM could alter AP morphology in substantia nigra and elsewhere in the brain (Bazzazi et al., 2013).

#### ApoCaM $P_O$ Modulation Extends to $\text{Na}_v$ Channels

The marked apoCaM modulation of  $\text{Ca}_v1.3$  gave reason to wonder whether this scheme might generalize to other ion channels. In particular, voltage-gated Na channels ( $\text{Na}_v$ ) have recently been shown to exhibit CaM-mediated CDI that appears remarkably similar to that in  $\text{Ca}_v$  channels (Ben-Johny et al., 2014). Moreover, earlier experiments report that apoCaM binds the carboxyl tail of  $\text{Na}_v$  channels (Herzog et al., 2003), an interaction confirmed in Figure S7. Given the extensive role of  $\text{Na}_v$  channels in fast electrical conduction within brain, heart, and muscle (Hille, 1984), we tested for apoCaM modulatory effects in  $\text{Na}_v$  channels. As alanine substitutions in the IQ domain of skeletal muscle



(legend on next page)

Na<sub>v</sub>1.4 channels have been shown to both reduce CaM binding and decrease current density (Herzog et al., 2003), we undertook direct single-molecule  $P_O$  measurements on this particular channel isoform.

To test for apoCaM modulatory effects, we compared the single-channel activity of wild-type Na<sub>v</sub>1.4 (which avidly binds apoCaM at baseline) with that of a mutant Na<sub>v</sub>1.4<sub>IQ/AA</sub> exhibiting weakened apoCaM affinity via IQ to AA substitution within the IQ domain (Figure S7). Wild-type recombinant Na<sub>v</sub>1.4 channels exhibited frequent stochastic openings of millisecond duration (Figure 7A). Normalizing the ensemble average of many such records (by unitary current  $i$  and number of channels  $N$ ) yields a robust  $P_O$  waveform that peaks at 0.5 (Figure 7B). This outcome is confirmed by plots of peak  $P_O$  versus step potential (Figure 7C), averaged from multiple patches. By contrast, Na<sub>v</sub>1.4<sub>IQ/AA</sub> channels might often lack apoCaM at baseline. Fitting with a mechanism where such channels would be reluctant to open, corresponding single-molecule records display a sparser pattern of activity with briefer openings (Figure 7D). The ensemble average explicitly confirms this impression, yielding a diminutive  $P_O$  waveform (Figure 7E) and  $P_O$ -V relation (Figure 7F). Still, this reduced opening could be an intrinsic effect of mutation, rather than of lacking apoCaM. To exclude the former possibility, we strongly coexpressed CaM with Na<sub>v</sub>1.4<sub>IQ/AA</sub> channels, a maneuver that should restore apoCaM binding via mass action. Reassuringly, corresponding single-molecule records again exhibit robust activity (Figure 7G), and peak  $P_O$  is rescued to near wild-type levels (Figures 7H and 7I), confirming a primary action of apoCaM to elevate  $P_O$ . These data therefore support conservation of apoCaM modulation of  $P_O$  in both Ca<sub>v</sub> and Na<sub>v</sub> channel superfamilies. As such, like the arrangement for Ca<sub>v</sub>1.3 channels, we propose that Na<sub>v</sub>1.4 channels have the potential to reside within one of three configurations (Figure 7J): low  $P_O$  configuration *E* lacking apoCaM; high  $P_O$  configuration *A* bound to apoCaM; and low  $P_O$  configuration *I* bound to Ca<sup>2+</sup>/CaM. Each configuration may elaborate distinct Na currents upon step depolarization (Figure 7J, bottom subpanels).

## DISCUSSION

Apocalmodulin has been traditionally viewed as playing a secondary role to Ca<sup>2+</sup>/calmodulin for effectuating molecular function (Alberts et al., 1994). More recently, however, there has been growing awareness that apoCaM serves many roles (Jurado et al., 1999). Here, we reveal that apoCaM itself prominently regulates both voltage-gated Ca<sup>2+</sup> and Na channels.

ApoCaM binding to these channels enhances opening several-fold, matching the strongest forms of ion-channel regulation. This effect may unify understanding of a vast array of channel variants and channelopathic mutations that modulate channel affinity for apoCaM. New avenues are thus opened for understanding and manipulating related diseases.

Before turning to broader ramifications, two enabling methodological advances merit attention. First, low-noise single-channel measurements permit direct observation of quantized regulatory phenomena (Figure 2), crucial to deducing mechanism. Second, chemical-dimerizer-based step generation of perimembrane CaM furnishes powerful means to observe CaM-regulatory events in real time within single cells, excluding ambiguities of data drawn from multiple cells and methods. Importantly, a prior strategy for elevating perimembranous CaM requires kinase activation (Yang et al., 2013), potentially complicating discernment of CaM-specific actions. Moreover, our study illustrates the capability of a step generator to resolve biological signal bifurcation upon the binding of a single molecule (apoCaM imparting both an immediate boost in  $P_O$  and subsequent CDI); such mechanisms are difficult to prove by customary steady-state methods. Indeed, the overall approach (Figure 3D) mirrors the phase-plane analysis of electronics, highlighting synergy between biological and electrical network analysis (Jack et al., 1975). Biological signal generators and analysis, based not only on perfusable ligands (Spencer et al., 1993) but also on light activation (Hahn and Kuhlman, 2010; Kennedy et al., 2010; Yazawa et al., 2009), may aid future understanding of other signaling systems.

Mechanistic advances for Ca<sup>2+</sup> channels are 3-fold. First, we discover that apoCaM binding to Ca<sup>2+</sup> channels strongly elevates  $P_O$  by up to 7-fold, before the onset of CDI. At least 2-fold increases of peak current were routinely seen in individual cells undergoing enrichment of apoCaM by rapamycin (Figure 4), but this enhancement is likely a lower bound imposed by limitations of apoCaM recruitment via chemical dimerization (Figure 4B). Using modal analysis of single channels (e.g., Figure 2G), 7-fold augmentation of  $P_O$  can be directly deduced. Additionally, the quantitative adherence of all variants to a single line in Figure 5D independently supports this 7-fold  $P_O$  modulatory range. That said, the extent of  $P_O$  regulation by apoCaM rivals the upregulation of L type Ca<sup>2+</sup> channels by adrenergic stimulation (Miriya et al., 2008), the prototypic modulatory system for fight-or-flight responses (Tsien et al., 1986). Second, we unveil an intimate connection between the modulation of  $P_O$  and CDI, where the binding of one and the same apoCaM to channels brings not only the ability to undergo CDI as previously reported

### Figure 7. ApoCaM Modulates $P_O$ of Na<sub>v</sub>1.4 Channels

- (A) Single-molecule records of wild-type Na<sub>v</sub>1.4 channels transiently expressed in HEK cells, with only endogenous CaM.  
 (B)  $P_O$  waveform obtained by normalizing ensemble average of >100 records by unitary current  $i$  and number of channels  $N$ .  
 (C) Plot of peak  $P_O$  versus step potential (from -90 mV holding potential), averaged over multiple patches. Error bars are  $\pm$  SEM.  
 (D) Single-channel records for Na<sub>v</sub>1.4 channels containing IQ to AA substitution (Na<sub>v</sub>1.4<sub>IQ/AA</sub>). Channels are coexpressed with the CaM chelator, BSCaM<sub>IQ</sub>, to minimize free CaM levels (Liu et al., 2010).  
 (E and F) Corresponding  $P_O$  waveform (E) and  $P_O$ -V relation (F). See also Figure S7.  
 (G) Single-channel traces for Na<sub>v</sub>1.4<sub>IQ/AA</sub> paired with overexpressed CaM.  
 (H and I) Corresponding  $P_O$  waveform (H) and  $P_O$ -V relation (I) both restored to near wild-type levels.  $P_O$ -V relations averaged from  $n = 5$ -8 patches each. Error bars, SEM.  
 (J) Top, proposed Na<sub>v</sub> configurations with respect to CaM. Bottom, simulated Na<sub>v</sub> currents for configurations above.

(Bazzazi et al., 2013; Ben-Johny et al., 2013; Liu et al., 2010) but also the aforementioned increase of initial  $P_O$ . Intriguingly, the  $P_O$  of channels lacking CaM (Figure 5E, configuration E) seems equivalent to that of channels that have undergone CDI (configuration I); in particular,  $P_E \sim P_I \sim 0.051$ . This outcome is visually confirmed in Figure 4 by the invariance of steady-state current after 300 ms depolarization during rapamycin (see exemplar traces). CDI may thus represent a relinquishing of the initial apoCaM enhancement of  $P_O$ . For reference, configurations A and I in Figure 5E explicitly correspond to proposed molecular arrangements in a prior publication (respectively, Figures 8b and 8c in Ben-Johny et al., 2013). Third, the spectrum of  $P_O$  and CDI properties of  $\text{Ca}_v1.3$  variants (Figure 1A) can now be unified by a single molecular effect—customization of channel binding to apoCaM (Figure 5E). Notably, beyond this specific effect, the properties of variant channels seem largely equivalent once apoCaM becomes bound or unbound. This conclusion is supported by the adherence of all tested variants to a single relation in Figure 5D. One nuance of this unified view may be that the voltage dependence of activation appears subtly different for a variant with an extended DCT that lacks apoCaM (Figures 1E, S1E, and S1F).

The biological implications of these mechanisms are considerable. In particular, the apoCaM affinities of many editing and splice variants are such that natural fluctuations in ambient CaM influence the distribution of channels between pools lacking or armed with apoCaM (Bazzazi et al., 2013; Liu et al., 2010). In switching between pools, we now know that  $P_O$  and CDI will be coordinately regulated (Figures 5E and 5F). Furthermore, variants tune not only the midpoint sensitivity to apoCaM at steady state but also the kinetic response to changes in apoCaM (cf., Figures 4D, 4E, and 4F), a property now discernible via CaM step generation. Indeed, it will be important to explore the sequelae of these distinctive kinetic and steady-state properties on  $\text{Ca}^{2+}$  homeostasis and dysfunction, given CaM variation in physiological and disease conditions (Bezprozvanny, 2009; Black et al., 2004; Bossuyt and Bers, 2013; Chafouleas et al., 1982; Ikeda et al., 2009; Lesnick et al., 2007; Yacoubian et al., 2008). Specifically, given the marked broadening of APs in substantia nigral neurons (Figure 6), it is tempting to speculate that elevated apoCaM predisposes for  $\text{Ca}^{2+}$ -related neurodegeneration in Parkinson's. Similar modulatory scenarios may pertain throughout the  $\text{Ca}_v1$ -2 superfamily (Ben-Johny and Yue, 2014), with corresponding biomedical implications. Finally, the mechanisms revealed here (Figures 5E) sharpen distinctions between CaM abnormalities relating to  $\text{Ca}^{2+}$ /CaM versus apoCaM dysfunction; for example, recently reported CaM missense mutations associated with long-QT syndrome are likely to selectively inhibit transitions into configuration I of  $\text{Ca}_v$  channels (in Figure 5E), while allowing normal access to configuration A via maintained binding of  $\text{Ca}^{2+}$ -free mutant CaMs (Lim-pitikul et al., 2014).

The extension of like mechanisms to other ion-channel families holds the broadest implications. Only recently have Na channels been shown to exhibit CaM-mediated CDI with similarity to  $\text{Ca}_v$  channels (Ben-Johny et al., 2014). This likeness is now significantly generalized by our finding that apoCaM also robustly amplifies  $P_O$  of  $\text{Na}_v1.4$  (Figure 7). This conserved

modulation in Na channels then suggests that channelopathic disease mutations (Lossin, 2009; Schroeter et al., 2010), RNA editing (Song et al., 2004), and alternative splicing (Lossin, 2009) could all alter apoCaM binding and thereby  $P_O$ . The consequences may be extensive, as the  $\text{Na}_v1.1$ -1.9 superfamily governs excitability in brain, heart, and skeletal muscle (Hille, 1984), and related diseases encompass epilepsy, autism, pathological pain, cardiac arrhythmias, and skeletal muscle myotonias (Lossin, 2009; Schroeter et al., 2010). More broadly, numerous other transport molecules bind apoCaM (Bosanac et al., 2005; Saimi and Kung, 2002; Samsó and Wagenknecht, 2002; Vocke et al., 2013; Wen and Levitan, 2002; Xia et al., 1998). Thus, apocalmodulin promises widespread ion-channel regulation whose scope and stature seem likely to proliferate.

## EXPERIMENTAL PROCEDURES

### Molecular Biology

$\text{Ca}_v1.3_S$  and  $\text{Ca}_v1.3_L$  are identical to previously published rat  $\text{Ca}_v1.3\Delta$  (AF370009.1) and rat  $\text{Ca}_v1.3\Delta$  with human long distal carboxyl tail (NM000718), respectively (Liu et al., 2010).  $\text{Ca}_v1.3_S$  editing/splice variants and apoCaM mutations are the same as those previously published (Bazzazi et al., 2013; Ben-Johny et al., 2013). Lyn-GFP-FRB construct is the same as previously published, and YFP-FKBP-CaM was generated from YFP-FKBP-PI(4)P5K (Ueno et al., 2011). Standard cloning and PCR-based strategies for generating  $\text{Ca}_v$  variants and FKBP-CaM clones are detailed in Extended Experimental Procedures.

### Whole-Cell Electrophysiology

Voltage-clamp and current-clamp whole-cell recording were performed using an Axopatch 200A amplifier. Data were collected and analyzed using custom MATLAB software (Mathworks). Details of recording conditions and recipes for internal and external solutions are specified in Extended Experimental Procedures.

### Single-Channel Electrophysiology

Single-channel recordings were performed in the on-cell configuration, using established methods from our laboratory (Tay et al., 2012). To reduce noise, patch pipettes were pulled from ultra-thick-walled borosilicate glass (BF200-116-10, Sutter Instruments) and coated with Sylgard. Recording conditions, data analysis, and recipes for internal and external solutions are provided in Extended Experimental Procedures.

### Rapamycin Experiments

Whole-cell currents were recorded for 100 s with regular external solution flowing at 2 ml/min. At 100 s, flow of regular solution was stopped, and flow of the same external containing 200 nM rapamycin was started, triggering dimerization of FRB and FKBP tags that then elevated perimembranous CaM. Flow rates were carefully matched between lines prior to experiments.

### Confocal Optical Imaging

Fluorescence images were captured at 20 s intervals, before and after bath application of 200 nM rapamycin. Images were recorded with Olympus Fluoview FV300 and Zeiss LSM710 laser scanning confocal microscopes. Images were analyzed using MATLAB and ImageJ. Details of experimental set-up and data analysis are provided in Extended Experimental Procedures.

### SNc Computer Simulation

AP waveforms for substantia nigra dopaminergic neurons were simulated using MATLAB 2010b (Mathworks) based on published models. Details of the model are included in Extended Experimental Procedures and Table S2.

### SNc DA Neuron Culture

SNc neurons were isolated from mice expressing GFP under the tyrosine hydroxylase promoter (TH-GFP) (GENSAT; Rockefeller University) (Gong et al.,



2003). Experimental procedures and solution recipes are included in [Extended Experimental Procedures](#).

## SUPPLEMENTAL INFORMATION

Supplemental Information includes Extended Experimental Procedures, seven figures, and two tables and can be found with this article online at <http://dx.doi.org/10.1016/j.cell.2014.09.047>.

## AUTHOR CONTRIBUTIONS

P.J.A. performed  $\text{Ca}_v$  channel experiments and data analysis. M.B.-J. created mutant channels and undertook  $\text{Na}_v$  experiments and analysis. P.J.A., M.B.-J., and D.T.Y. developed the single-versus-multiple-CaM model. M.B.-J. analyzed fluorescence imaging data and built the SN DA neuron model. I.E.D. supported single-channel data acquisition and analysis and AP analysis. T.I. helped develop the FKBP and FRB CaM system. P.J.A., M.B.-J., and D.T.Y. conceived the project and refined experimental design. P.J.A. and D.T.Y. wrote the paper.

## ACKNOWLEDGMENTS

We thank Hojjat Bazzazi and Philemon Yang for providing some  $\text{Ca}_v1.3$  variants,  $\text{Ca}^{2+}$  Signals Lab members for valuable comments, and Wanjun Yang for technical support. This work was supported by grants from the NINDS (to D.T.Y.), NHLBI (D.T.Y.), NIMH (M.B.-J.), and Parkinson Society Canada (P.J.A.).

Received: May 19, 2014

Revised: July 25, 2014

Accepted: September 26, 2014

Published: October 23, 2014

## REFERENCES

- Alberts, B., Bray, D., Lewis, J., Raff, M., Roberts, K., and Watson, J.D. (1994). *Molecular Biology of the Cell*, Third Edition (New York, London: Garland Publishing, Inc.).
- Bazzazi, H., Ben-Johny, M., Adams, P.J., Soong, T.W., and Yue, D.T. (2013). Continuously tunable  $\text{Ca}^{2+}$  regulation of RNA-edited  $\text{Ca}_v1.3$  channels. *Cell Rep* 5, 367–377.
- Bean, B.P. (2007). Neurophysiology: stressful pacemaking. *Nature* 447, 1059–1060.
- Ben-Johny, M., Yang, P.S., Bazzazi, H., and Yue, D.T. (2013). Dynamic switching of calmodulin interactions underlies  $\text{Ca}^{2+}$  regulation of  $\text{Ca}_v1.3$  channels. *Nat. Commun.* 4, 1717.
- Ben-Johny, M., Yang, P.S., Niu, J., Yang, W., Joshi-Mukherjee, R., and Yue, D.T. (2014). Conservation of  $\text{Ca}^{2+}$ /calmodulin regulation across Na and  $\text{Ca}^{2+}$  channels. *Cell* 157, 1657–1670.
- Ben-Johny, M., and Yue, D.T. (2014). Calmodulin regulation (calmodulation) of voltage-gated calcium channels. *J. Gen. Physiol.* 143, 679–692.
- Bers, D.M., and Grandi, E. (2009). Calcium/calmodulin-dependent kinase II regulation of cardiac ion channels. *J. Cardiovasc. Pharmacol.* 54, 180–187.
- Bezprozvanny, I. (2009). Calcium signaling and neurodegenerative diseases. *Trends Mol. Med.* 15, 89–100.
- Black, D.J., Tran, K.K., and Persechini, A. (2004). Monitoring the total available calmodulin concentration in intact cells over the physiological range in free  $\text{Ca}^{2+}$ . *Cell Calcium* 35, 415–425.
- Bock, G., Gebhart, M., Scharinger, A., Jangsangthong, W., Busquet, P., Pogiani, C., Sartori, S., Mangoni, M.E., Sinnegger-Brauns, M.J., Herzig, S., et al. (2011). Functional properties of a newly identified C-terminal splice variant of  $\text{Ca}_v1.3$  L-type  $\text{Ca}^{2+}$  channels. *J. Biol. Chem.* 286, 42736–42748.
- Bosanac, I., Yamazaki, H., Matsu-Ura, T., Michikawa, T., Mikoshiba, K., and Ikura, M. (2005). Crystal structure of the ligand binding suppressor domain of type 1 inositol 1,4,5-trisphosphate receptor. *Mol. Cell* 17, 193–203.
- Bossuyt, J., and Bers, D.M. (2013). Visualizing CaMKII and CaM activity: a paradigm of compartmentalized signaling. *J. Mol. Med.* 91, 907–916.
- Cardozo, D.L., and Bean, B.P. (1995). Voltage-dependent calcium channels in rat midbrain dopamine neurons: modulation by dopamine and GABAB receptors. *J. Neurophysiol.* 74, 1137–1148.
- Chafouleas, J.G., Bolton, W.E., Hidaka, H., Boyd, A.E., 3rd, and Means, A.R. (1982). Calmodulin and the cell cycle: involvement in regulation of cell-cycle progression. *Cell* 28, 41–50.
- Chan, C.S., Guzman, J.N., Ilijic, E., Mercer, J.N., Rick, C., Tkatch, T., Meredith, G.E., and Surmeier, D.J. (2007). ‘Rejuvenation’ protects neurons in mouse models of Parkinson’s disease. *Nature* 447, 1081–1086.
- Chao, S.H., Suzuki, Y., Zysk, J.R., and Cheung, W.Y. (1984). Activation of calmodulin by various metal cations as a function of ionic radius. *Mol. Pharmacol.* 26, 75–82.
- Christel, C.J., Cardona, N., Mesirca, P., Herrmann, S., Hofmann, F., Striessnig, J., Ludwig, A., Mangoni, M.E., and Lee, A. (2012). Distinct localization and modulation of  $\text{Ca}_v1.2$  and  $\text{Ca}_v1.3$  L-type  $\text{Ca}^{2+}$  channels in mouse sinoatrial node. *J. Physiol.* 590, 6327–6342.
- Erickson, M.G., Liang, H., Mori, M.X., and Yue, D.T. (2003). FRET two-hybrid mapping reveals function and location of L-type  $\text{Ca}^{2+}$  channel CaM preassociation. *Neuron* 39, 97–107.
- Evans, R.M., and Zamponi, G.W. (2006). Presynaptic  $\text{Ca}^{2+}$  channels—integration centers for neuronal signaling pathways. *Trends Neurosci.* 29, 617–624.
- Fallon, J.L., Baker, M.R., Xiong, L., Loy, R.E., Yang, G., Dirksen, R.T., Hamilton, S.L., and Quiocho, F.A. (2009). Crystal structure of dimeric cardiac L-type calcium channel regulatory domains bridged by  $\text{Ca}^{2+}$  calmodulins. *Proc. Natl. Acad. Sci. USA* 106, 5135–5140.
- Gong, S., Zheng, C., Doughty, M.L., Losos, K., Didkovsky, N., Schambra, U.B., Nowak, N.J., Joyner, A., Leblanc, G., Hatten, M.E., and Heintz, N. (2003). A gene expression atlas of the central nervous system based on bacterial artificial chromosomes. *Nature* 425, 917–925.
- Grace, A.A., and Bunney, B.S. (1984). The control of firing pattern in nigral dopamine neurons: single spike firing. *J. Neurosci.* 4, 2866–2876.
- Hahn, K.M., and Kuhlman, B. (2010). Hold me tightly LOV. *Nat. Methods* 7, 595–597, 597.
- Herzog, R.I., Liu, C., Waxman, S.G., and Cummins, T.R. (2003). Calmodulin binds to the C terminus of sodium channels  $\text{Na}_v1.4$  and  $\text{Na}_v1.6$  and differentially modulates their functional properties. *J. Neurosci.* 23, 8261–8270.
- Hess, P., Lansman, J.B., and Tsien, R.W. (1984). Different modes of Ca channel gating behaviour favoured by dihydropyridine Ca agonists and antagonists. *Nature* 311, 538–544.
- Hille, B. (1984). *Ionic Channels of Excitable Membranes* (Sunderland, MA: Sinauer Associates).
- Huang, H., Tan, B.Z., Shen, Y., Tao, J., Jiang, F., Sung, Y.Y., Ng, C.K., Raida, M., Köhr, G., Higuchi, M., et al. (2012). RNA editing of the IQ domain in  $\text{Ca}_v1.3$  channels modulates their  $\text{Ca}^{2+}$ -dependent inactivation. *Neuron* 73, 304–316.
- Hui, A., Ellinor, P.T., Krizanov, O., Wang, J.J., Diebold, R.J., and Schwartz, A. (1991). Molecular cloning of multiple subtypes of a novel rat brain isoform of the  $\alpha 1$  subunit of the voltage-dependent calcium channel. *Neuron* 7, 35–44.
- Ikeda, S., He, A., Kong, S.W., Lu, J., Bejar, R., Bodyak, N., Lee, K.H., Ma, Q., Kang, P.M., Golub, T.R., and Pu, W.T. (2009). MicroRNA-1 negatively regulates expression of the hypertrophy-associated calmodulin and Mef2a genes. *Mol. Cell. Biol.* 29, 2193–2204.
- Imredy, J.P., and Yue, D.T. (1994). Mechanism of  $\text{Ca}^{2+}$ -sensitive inactivation of L-type  $\text{Ca}^{2+}$  channels. *Neuron* 12, 1301–1318.
- Jack, J.J.B., Noble, D., and Tsien, R.W. (1975). *Electric Current Flow in Excitable Cells* (Oxford, England: Clarendon Press).
- Jurado, L.A., Chockalingam, P.S., and Jarrett, H.W. (1999). Apocalmodulin. *Physiol. Rev.* 79, 661–682.

- Kennedy, M.J., Hughes, R.M., Peteya, L.A., Schwartz, J.W., Ehlers, M.D., and Tucker, C.L. (2010). Rapid blue-light-mediated induction of protein interactions in living cells. *Nat. Methods* 7, 973–975.
- Kim, E.Y., Rumpf, C.H., Van Petegem, F., Arant, R.J., Findeisen, F., Cooley, E.S., Isacoff, E.Y., and Minor, D.L., Jr. (2010). Multiple C-terminal tail  $\text{Ca}^{2+}$ /CaMs regulate  $\text{Ca}_v1.2$  function but do not mediate channel dimerization. *EMBO J.* 29, 3924–3938.
- Lesnick, T.G., Papapetropoulos, S., Mash, D.C., French-Mullen, J., Shehadeh, L., de Andrade, M., Henley, J.R., Rocca, W.A., Ahlskog, J.E., and Manganore, D.M. (2007). A genomic pathway approach to a complex disease: axon guidance and Parkinson disease. *PLoS Genet.* 3, e98.
- Limpitkul, W.B., Dick, I.E., Joshi-Mukherjee, R., Overgaard, M.T., George, A.L., Jr., and Yue, D.T. (2014). Calmodulin mutations associated with long QT syndrome prevent inactivation of cardiac L-type  $\text{Ca}^{2+}$  currents and promote proarrhythmic behavior in ventricular myocytes. *J. Mol. Cell. Cardiol.* 74, 115–124.
- Liu, X., Yang, P.S., Yang, W., and Yue, D.T. (2010). Enzyme-inhibitor-like tuning of  $\text{Ca}^{2+}$  channel connectivity with calmodulin. *Nature* 463, 968–972.
- Lossin, C. (2009). A catalog of SCN1A variants. *Brain Dev.* 31, 114–130.
- Luik, R.M., Wang, B., Prakriya, M., Wu, M.M., and Lewis, R.S. (2008). Oligomerization of STIM1 couples ER calcium depletion to CRAC channel activation. *Nature* 454, 538–542.
- Miriyala, J., Nguyen, T., Yue, D.T., and Colecraft, H.M. (2008). Role of  $\text{Ca}_v\beta$  subunits, and lack of functional reserve, in protein kinase A modulation of cardiac  $\text{Ca}_v1.2$  channels. *Circ. Res.* 102, e54–e64.
- Nedergaard, S. (1999). Regulation of size and excitability in substantia nigra compacta neurons: sensitivity to 4-aminopyridine. *J. Neurophysiol.* 82, 2903–2913.
- Obeso, J.A., Marin, C., Rodríguez-Oroz, C., Blesa, J., Benítez-Temiño, B., Mena-Segovia, J., Rodríguez, M., and Olanow, C.W. (2008). The basal ganglia in Parkinson's disease: current concepts and unexplained observations. *Ann. Neurol.* 64 (Suppl 2), S30–S46.
- Phua, S.C., Pohlmeier, C., and Inoue, T. (2012). Rapidly relocating molecules between organelles to manipulate small GTPase activity. *ACS Chem. Biol.* 7, 1950–1955.
- Pitt, G.S., Zühlke, R.D., Hudmon, A., Schulman, H., Reuter, H., and Tsien, R.W. (2001). Molecular basis of calmodulin tethering and  $\text{Ca}^{2+}$ -dependent inactivation of L-type  $\text{Ca}^{2+}$  channels. *J. Biol. Chem.* 276, 30794–30802.
- Puopolo, M., Raviola, E., and Bean, B.P. (2007). Roles of subthreshold calcium current and sodium current in spontaneous firing of mouse midbrain dopamine neurons. *J. Neurosci.* 27, 645–656.
- Saimi, Y., and Kung, C. (2002). Calmodulin as an ion channel subunit. *Annu. Rev. Physiol.* 64, 289–311.
- Samsó, M., and Wagenknecht, T. (2002). Apocalmodulin and  $\text{Ca}^{2+}$ -calmodulin bind to neighboring locations on the ryanodine receptor. *J. Biol. Chem.* 277, 1349–1353.
- Schroeter, A., Walzik, S., Blechschmidt, S., Haufe, V., Benndorf, K., and Zimmer, T. (2010). Structure and function of splice variants of the cardiac voltage-gated sodium channel  $\text{Na}_v1.5$ . *J. Mol. Cell. Cardiol.* 49, 16–24.
- Song, W., Liu, Z., Tan, J., Nomura, Y., and Dong, K. (2004). RNA editing generates tissue-specific sodium channels with distinct gating properties. *J. Biol. Chem.* 279, 32554–32561.
- Spencer, D.M., Wandless, T.J., Schreiber, S.L., and Crabtree, G.R. (1993). Controlling signal transduction with synthetic ligands. *Science* 262, 1019–1024.
- Suh, B.C., Inoue, T., Meyer, T., and Hille, B. (2006). Rapid chemically induced changes of  $\text{PtdIns}(4,5)\text{P}_2$  gate KCNQ ion channels. *Science* 314, 1454–1457.
- Tan, B.Z., Jiang, F., Tan, M.Y., Yu, D., Huang, H., Shen, Y., and Soong, T.W. (2011). Functional characterization of alternative splicing in the C terminus of L-type  $\text{Ca}_v1.3$  channels. *J. Biol. Chem.* 286, 42725–42735.
- Tay, L.H., Dick, I.E., Yang, W., Mank, M., Griesbeck, O., and Yue, D.T. (2012). Nanodomain  $\text{Ca}^{2+}$  of  $\text{Ca}^{2+}$  channels detected by a tethered genetically encoded  $\text{Ca}^{2+}$  sensor. *Nat. Commun.* 3, 778.
- Tsien, R.W., Bean, B.P., Hess, P., Lansman, J.B., Nilius, B., and Nowycky, M.C. (1986). Mechanisms of calcium channel modulation by beta-adrenergic agents and dihydropyridine calcium agonists. *J. Mol. Cell. Cardiol.* 18, 691–710.
- Ueno, T., Falkenburger, B.H., Pohlmeier, C., and Inoue, T. (2011). Triggering actin comets versus membrane ruffles: distinctive effects of phosphoinositides on actin reorganization. *Sci. Signal.* 4, ra87.
- Vocke, K., Dauner, K., Hahn, A., Ulbrich, A., Broecker, J., Keller, S., Frings, S., and Möhrlen, F. (2013). Calmodulin-dependent activation and inactivation of anoctamin calcium-gated chloride channels. *J. Gen. Physiol.* 142, 381–404.
- Wen, H., and Levitan, I.B. (2002). Calmodulin is an auxiliary subunit of KCNQ2/3 potassium channels. *J. Neurosci.* 22, 7991–8001.
- Xia, X.M., Fakler, B., Rivard, A., Wayman, G., Johnson-Pais, T., Keen, J.E., Ishii, T., Hirschberg, B., Bond, C.T., Lutsenko, S., et al. (1998). Mechanism of calcium gating in small-conductance calcium-activated potassium channels. *Nature* 395, 503–507.
- Xu, W., and Lipscombe, D. (2001). Neuronal  $\text{Ca}_v1.3\alpha(1)$  L-type channels activate at relatively hyperpolarized membrane potentials and are incompletely inhibited by dihydropyridines. *J. Neurosci.* 21, 5944–5951.
- Yacoubian, T.A., Cantuti-Castelvetri, I., Bouzou, B., Asteris, G., McLean, P.J., Hyman, B.T., and Standaert, D.G. (2008). Transcriptional dysregulation in a transgenic model of Parkinson disease. *Neurobiol. Dis.* 29, 515–528.
- Yang, T., He, L.L., Chen, M., Fang, K., and Colecraft, H.M. (2013). Bio-inspired voltage-dependent calcium channel blockers. *Nat Commun* 4, 2540.
- Yazawa, M., Sadaghiani, A.M., Hsueh, B., and Dolmetsch, R.E. (2009). Induction of protein-protein interactions in live cells using light. *Nat. Biotechnol.* 27, 941–945.